MACHINE SCIENCE

ISSN: 2227-6912
E-ISSN: 2790-0479

2023, № 2 Pages 5 – 19

THE EFFECTS OF PARTICLE SIZE AND TEMPERATURE ON THE STABILITY AND LOCAL STRUCTURAL EVOLUTIONS OF AMORPHOUS BULK AND NANOPARTICLES OF THE $FeNI_3$ ALLOYS

Amdulla MEKHRABOV[1,2,a*], Ece A. IRMAK[3,b], M. Vedat AKDENİZ[3,c]

[1]Novel Materials and Nanotechnologies Institute, Azerbaijan Technical University, Baku, Azerbaijan
[2]Faculty of Metallurgy and Materials Science, Department of Metallurgy and Materials Technologies, Azerbaijan Technical University, Baku, Azerbaijan
[3]Novel Alloy Design and Development Laboratory (NOVALAB), Department of Metallurgical and Materials Engineering, Middle East Technical University, Ankara, Türkiye

E-mail: *[a]*emdulla.mehrabov@aztu.edu.az*

http://dx.doi.org/10.61413/CEAD8914

Abstract: The effects of particle size (2-6 nm) and temperature (300-1900 K) on the stability and local structural evolutions of amorphous bulk and nanoparticles of the $FeNi_3$ alloys have been studied by using classical molecular dynamics (MD) simulation method combined with embedded atom model (EAM) in Large-scale Atomic/Molecular Massively Parallel Simulator (LAMMPS). The nanoparticles were obtained from the unstable amorphous bulk $FeNi_3$ alloys. MD simulations have been performed for glassy $FeNi_3$ intermetallic alloy by making use of pairwise interatomic interaction potentials and electron densities calculated via EAM method. The formation and evolution of structures and their stability have been analyzed at a wide temperature range (300-1900 K) by calculating radial distribution functions (RDF), interatomic distances (ID), coordination numbers (CN), core-to-surface concentration profiles, as well as Voronoi analysis. According to the results, although some deviations in the structural properties occurred during the heat treatment, the amorphous nanoparticles exhibited the same crystal structure and local atomic configuration with its bulk counterpart at room temperature.

Keywords: *Fe-Ni, Amorphous, Bulk and Nanoparticles, Modelling and Simulations, Molecular dynamics, Embedded atom model*

Introduction.

There is a growing research interest on the modeling and simulation of the magnetic nanoalloys, since the unique and sometimes superior chemical and physical properties of the nanoalloys can be tuned and, consequently, new structural motifs can be created by varying the type of constituent elements, atomic and magnetic ordering, as well as size and shape of the nanoparticles for several promising research and application area [1]. For new generation magnetic nanoalloys, it is important to predict structure-property relations in advance because of the complexity increased by the various structural and geometrical forms in addition to the size-dependent structure [2, 3]. Among the magnetic nanoalloys, Fe-Ni based magnetic nanoalloys have promising usage area in the diversified engineering applications, such as radar absorbing materials in aerospace and stealth industry, catalyst, and biomedical applications, due to their superior mechanical, electrical, optical and magnetic properties with high surface area [4-9]. However, there is not enough study regarding these usage areas of the Fe-Ni nanoalloys because of the concern of the agglomeration, oxidation, and degradation; therefore, it is essential to predict and determine the thermally stable size and shape of the nanoparticles [9]. Computer simulation techniques have been widely used to investigate structural properties of the Fe-Ni based bulk and nanostructured alloys for a long time. Atomic and magnetic

ordering, order-disorder and ferromagnetic-paramagnetic transformation characteristics and also interrelation between atomic and magnetic ordering phenomena in binary $FeNi_3$ and ternary Ni_3(Fe, Me) (Me= W, Mo, Cr, Mn, Nb, etc.) bulk intermetallics have been widely investigated in terms of classical theory of ordering and electronic theory of binary and multicomponent alloys in ab-initio pseudopotential approximation [10-16]. Although the first principle calculations on the Fe-Ni based alloys have been used to predict the properties from atomistic level [17, 18], the molecular dynamics simulations with many-body potentials are mainly preferred because of its applicability to the large systems having more than hundreds of atoms. However, to acquire accurate and efficient results from the molecular dynamics simulations, inter-atomic potential energy functions have a crucial effect [19].

Therefore, in this study, stability and local structural evolutions in amorphous intermetallic $FeNi_3$ nanoparticles with 2-6 nm particle size have been modeled and simulated for wide temperature range (from room temperature up to 1900 K) by means of EAM-MD simulation methods in Large-scale Atomic/Molecular Massively Parallel Simulator (LAMMPS).

Methodology

2.1. Pairwise interatomic interaction potentials calculations

EAM method is based on the density functional theory and it considers many-body interaction through the electron density of the systems. Therefore, EAM gives more accurate results than the pairwise interaction models with reasonable computational time for Fe-based systems [20-22]. According to EAM model [20], the energy of the system which consists of N-atoms can be expressed as,

$$E = \sum_i F_i(\rho_i) + \frac{1}{2}\sum_{ij} V_{ij}(r_{ij}) \tag{1}$$

where V_{ij} represents the pairwise interatomic interaction potentials between atoms i and j separated by distance of r_{ij} (in Eq. (1), i and j, regardless of the different type of atoms, represent any atoms), and F_i stands for the embedding energy to embed an atom i into a local site with electron density $\bar{\rho}_i$ and $\bar{\rho}_i$ can be calculated by using

$$\bar{\rho}_i = \sum_{i \neq j} \rho(r_{ij}) \tag{2}$$

with $\rho(r_{ij})$ being the electron density at the site of atom i arising from atom j at a distance r_{ij} away.

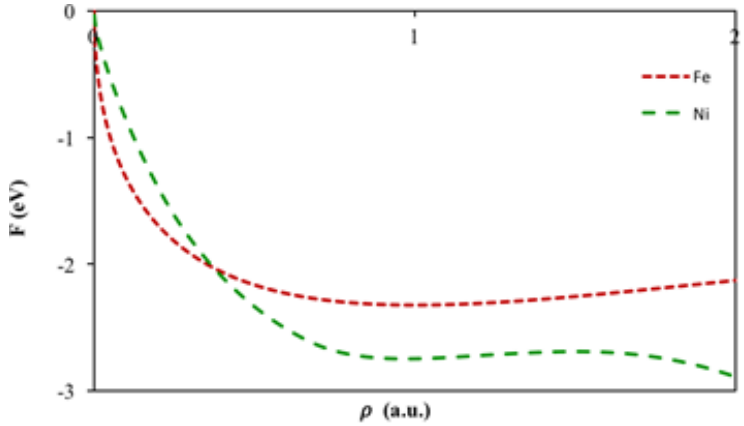

Figure 1. Embedding energy variation with electron density in $FeNi_3$ alloy

In this study, the EAM parameters that were determined in [20] have been used for calculations of the embedding energy variation with electron density and electron density dependence on interatomic separation distance in $FeNi_3$ alloy by means of LAMMPS program system, which are shown in Figs. 1 and 2, respectively.

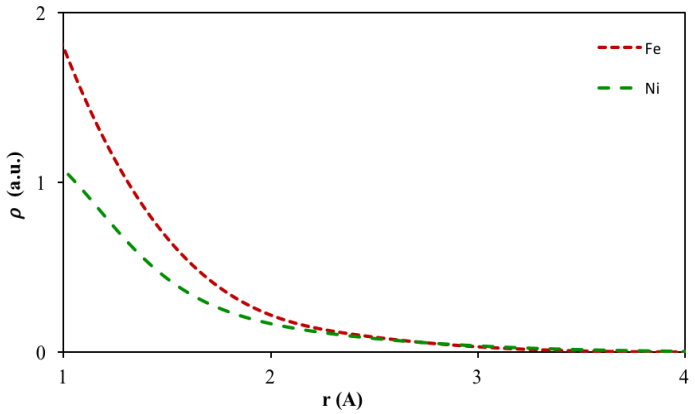

Figure. 2. Electron density dependence on interatomic separation distance in $FeNi_3$ alloy

Calculated pairwise interatomic interaction potentials variations with interatomic distance for Fe-Fe, Ni-Ni and Fe-Ni atomic pairs in FeNi alloy are presented in Fig. 3.

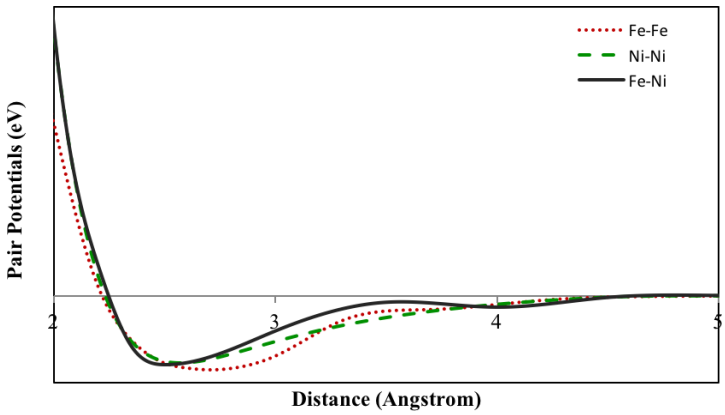

Figure 3. Pairwise interatomic interaction potentials variation with interatomic separation distance in $FeNi_3$ alloy

2.2. MD simulations of $FeNi_3$ nanoparticles

MD simulations have been performed by means of MedeA - LAMMPS molecular dynamics simulator program system, by using interatomic interaction potentials and electron densities calculated via EAM method. During solving the equation of motions of atoms in MD, Verlet algorithm was considered with Nose-Hoover thermostat and barostat. Among the ensembles typically used for molecular dynamics, namely the microcanonical (NVE), canonical (NVT) and isothermal–isobaric (NPT) ensembles, the NPT ensemble was applied in this study because it accurately describes experimental conditions by controlling temperature and pressure at the same time [23, 24].

$FeNi_3$ alloy is known to have a chemically ordered face-centered cubic (FCC) $L1_2$-type structure as shown in Fig 4.

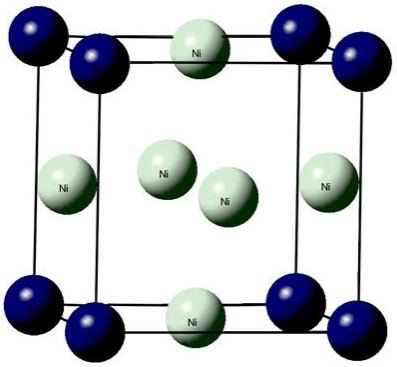

Figure 4. $AuCu_3$-type ordered ($L1_2$) FCC lattice of $FeNi_3$ alloys

The bulk form of $FeNi_3$ alloy, having 27436 atoms, was generated by repeating the $L1_2$ structured unit cell along [111] direction nineteen times. Firstly, the lattice parameter of $FeNi_3$ alloy was optimized and the alloy was relaxed at 0 K under the periodic boundary conditions. Then, the temperature was increased to 2600 K under 1 atm pressure directly with $5x10^5$ MD steps and the system waited for $5x10^4$ steps. 2600 K is higher than the melting temperature of alloy which was enough to homogenize the liquid structure. In order to obtain the amorphous bulk structure, the system was cooled down from 2600 K to 300 K by fast cooling ($2.3x10^{13}$ K/sec) and stabilized at room temperature. The time step was 1 fs and the motion of atoms was integrated by using Verlet algorithms. Non-periodic boundary condition was applied to simulate the amorphous bimetallic $FeNi_3$ NPs. Firstly, NPs was subtracted from the simulated amorphous bulk alloy, Fig. 5.

Then, the subtracted NPs was melted and equilibrated at 1900 K in order to remove local atomic configurations from the solid phase. Finally, the temperature of NPs was decreased to room temperature, gradually. To obtain accurate results from molecular dynamics simulations, the temperature of the amorphous NPs was decreased with the same cooling rate ($2x10^{12}$ K/sec) as bulk alloys and equilibrate the system at each stage by waiting for 10 nanoseconds. The simulations of the amorphous NPs were conducted for 2 nm, 4 nm and 6 nm diameters (the total number of atoms are 368, 2913 and 9784, respectively. The heat-treated amorphous $FeNi_3$ nanoparticles were illustrated by using VMD molecular graphics program.

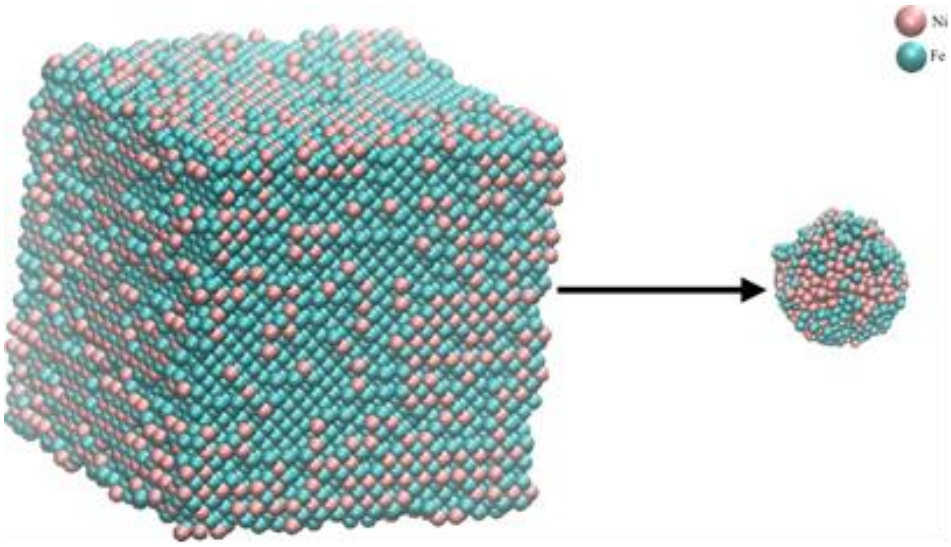

Figure 5. Extraction of NPs from bulk amorphous $FeNi_3$ alloy

Results and discussions

3.1. Radial distribution functions (RDF) for the bulk $FeNi_3$ alloy

Before the investigation of the structural evolution of the $FeNi_3$ bulk system, the lattice parameter was optimized. In this regard, crystal structures were generated with different lattice parameters (from 3 Å to 4 Å). Then, the systems were minimized by conjugate gradient method in MD, and the total energies of the crystal structures were calculated. Afterward, the crystal structure owing to the minimum total energy was obtained with the lattice parameter, a=3.46 Å. Then, the input file of the $FeNi_3$ bulk system was prepared according to the minimized lattice parameter, a=3.46 Å. The total energy change with respect to the various lattice parameters is shown in Figure 6.

To obtain the amorphous bulk structure, the system was cooled from 2600 K to 300 K by fast cooling with $2.3x10^{13}$ K/sec cooling rate. The volume changes during heating and fast cooling for the bulk $FeNi_3$ alloy is shown in Figure 7.

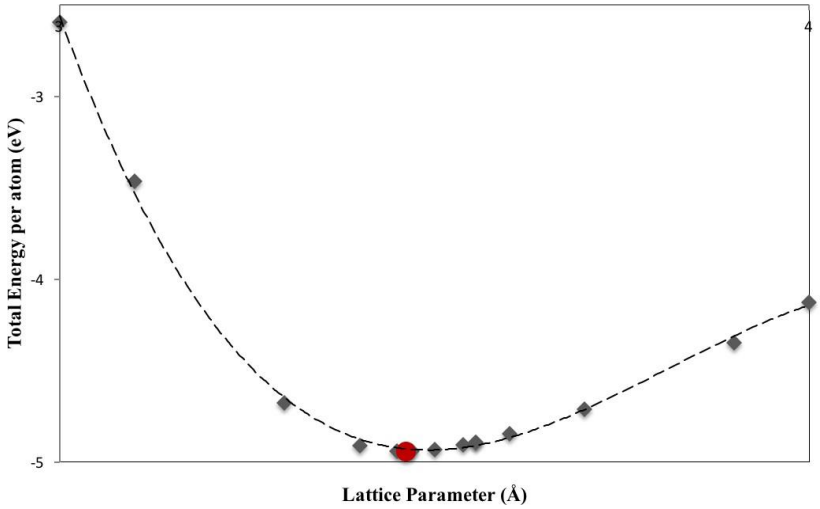

Figure 6. The total energy variation with lattice parameters of $FeNi_3$ alloy

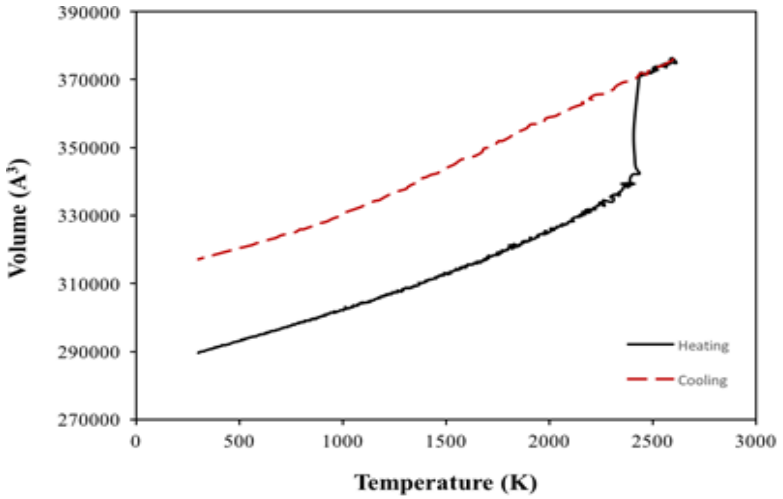

Figure 7. The volume change during heating and fast cooling processes of the $FeNi_3$ alloy

During the heating process, there was a sudden jump in the volume curve which is the sign of the melting. However, we did not observe any sudden change in the volume during fast cooling with $2.3x10^{13}$ K/sec rate, which indicated that no crystallization occurred and the amorphous structure was

preserved at room temperature. Also, this amorphous structure was proven by the RDFs which is illustrated in Figure 8.

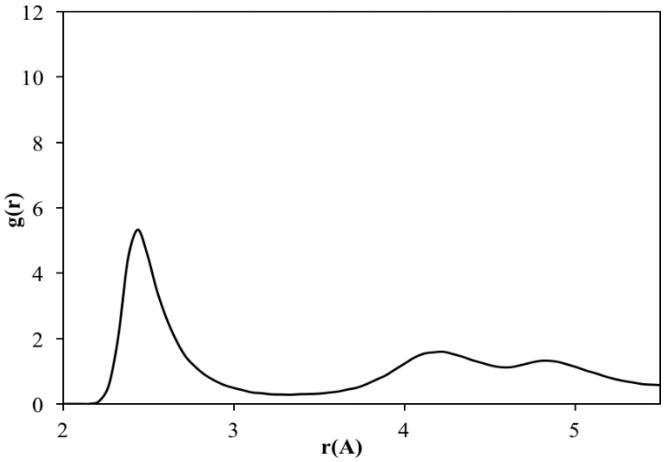

Figure 8. RDF of the $FeNi_3$ amorphous bulk alloy

The calculated partial coordination numbers and nearest-neighbor distances of the amorphous bulk $FeNi_3$ alloy are tabulated in Table 1. The total coordination number of the bulk amorphous $FeNi_3$ alloy obtained from the RDF was 13.2.

Table 1. The partial coordination numbers and nearest-neighbor distance of amorphous bulk $FeNi_3$ alloy

Amorphous bulk $FeNi_3$ alloy	N_{Fe-Fe}	N_{Fe-Ni}	N_{Ni-Ni}	d_{Fe-Fe}	d_{Fe-Ni}	d_{Ni-Ni}
(EAM-MD method)	4.3	9.0	10.2	2.5	2.4	2.4

3.2 RDF for the amorphous $FeNi_3$ NPs

RDF dependences on temperature for 2 nm, 4 nm and 6 nm amorphous nanoparticle are given in Figures 9 (a), (b) and (c), respectively. The nanoparticle with the diameter equal to 2 nm consists of 368 atoms in total, with 112 iron atoms and 256 nickel atoms. To determine the temperature effect on the structural evolution of the nanoparticles, the systems were cooled from 1900 K to 300 K by 200 K interval.

According to Figure 9 (a), we clearly observed that, at high temperatures, there was an absence of order between atoms, but the first peaks were always clear at high temperatures. As the temperature decreased, the first peak steepened and the structure between the first neighbors approached to the crystalline phase, even though the amorphous and disordered phase remained between the second and third neighbors of the atoms.

The nanoparticle having the diameter equal to 4 nm consists of 2913 atoms in total, with 761 iron atoms and 2152 nickel atoms. In Figure 9 (b), even though the first peaks were always observed during the cooling process, the disordered structure was mainly preserved until 900 K. After that point, the second and third peaks appeared, and at 300 K, mainly, a crystal structure was obtained.

It is evident that all the peaks at 300 K have a broadened shape but the first, second and third peaks located at the same positions as it was found for crystalline counterpart. This means the inner side of the amorphous 4 nm nanoparticle (until 3^{rd} nearest neighbor distance) mostly transformed to the crystal structure at room temperature although the remaining part preserved its disordered amorphous structure. Throughout the amorphous to the crystalline transition process, lattice

parameter decreased from 3.612 Å at 900 K and reached to 3.5 Å at 300 K that is the same value with the lattice parameter of the initially crystalline nanoparticle with 4 nm diameter.

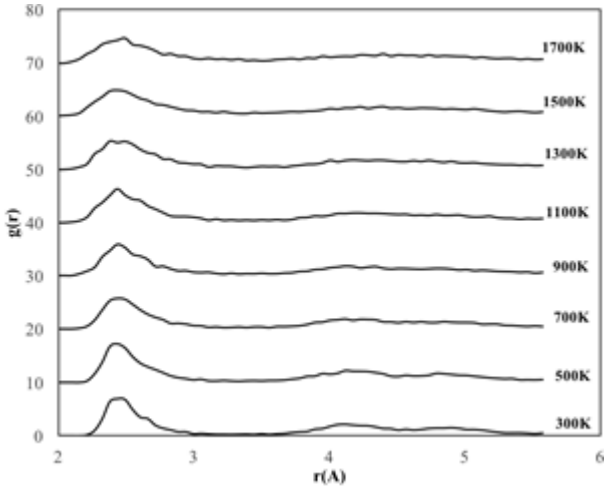

a)

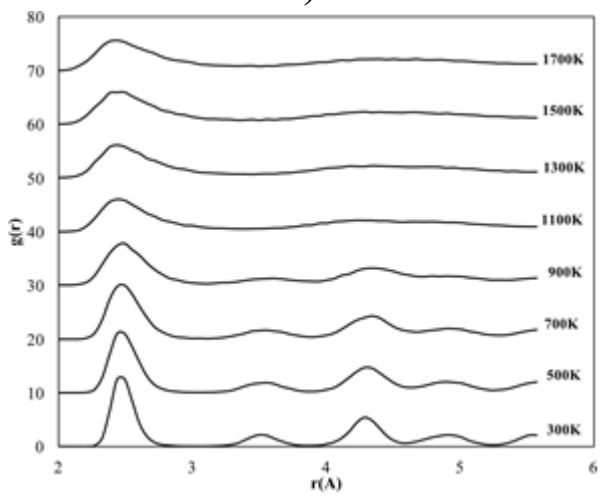

b)

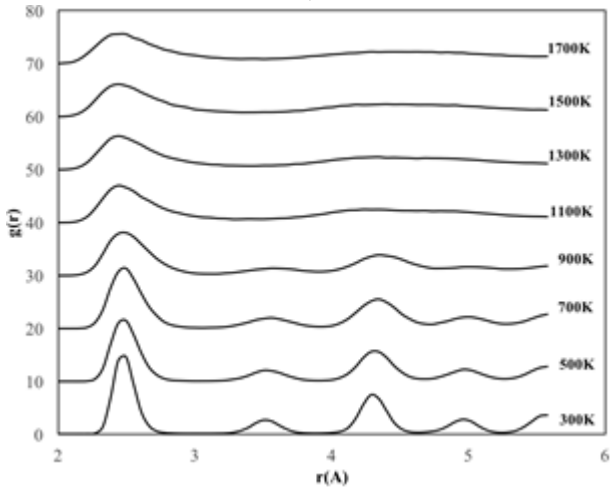

c)

Figure 9. RDF dependences on temperature for (a) 2 nm, (b) 4 nm and (c) 6 nm amorphous nanoparticles

The amorphous nanoparticle with 6 nm diameter includes 2450 Fe atoms and 7334 Ni atoms (9784 atoms in total). Like 4 nm amorphous nanoparticle, the peaks started to appear and the valley

between the peaks became deeper at 900 K, but the amorphous-to-crystalline transformation occurred in a faster and sharper way. At 300 K, the first and the second peak of the overall radial distribution of the initially amorphous 6 nm nanoparticle had almost the same height and width with the RDF of 6 nm crystalline nanoparticle, Figure 9 (c).

Although the other peaks were located in the same position, they had a broader shape compared to the peaks in the RDF of the initially crystalline nanoparticle with 6 nm. This means that the 6 nm nanoparticle, which owned amorphous phase at the beginning, completely transformed to the crystalline phase, even though the final structure has not been as compact as the structure of the initially crystalline nanoparticle with the 6 nm diameter at room temperature. Moreover, during the cooling process, the lattice parameter of the 6 nm particle changed from the 3.556 Å at 900 K, where crystallization started, to 3.5 Å at room temperature which is consistent with the lattice parameter of the initially crystalline nanoparticle and the value stated in the literature [25].

Overall, we observed clearly that, at high temperatures, there was an absence of an order for all initially amorphous nanoparticles. From the RDF graphs of the 2 nm nanoparticles, it has been seen that amorphous structure was preserved during the cooling process even at 300 K. On the other hand, in the RDF figures of the nanoparticles with 4 nm and 6 nm diameter, there was a transition from amorphous phase to the crystal structure at lower temperatures, and 300 K, the complete crystalline structure was obtained in 6 nm nanoparticle with 3.5 Å lattice constant. Although at 300 K, the lattice parameter of both 6 nm and 4 nm nanoparticles reached to 3.5 Å value, the variation in lattice constant of the nanoparticle with 4 nm diameter was higher than 6 nm diameter because of the size effect on the lattice parameter [26].

Moreover, the coordination number change of the 2 nm, 4 nm and 6 nm amorphous nanoparticles with respect to temperature is illustrated in Figure 10.

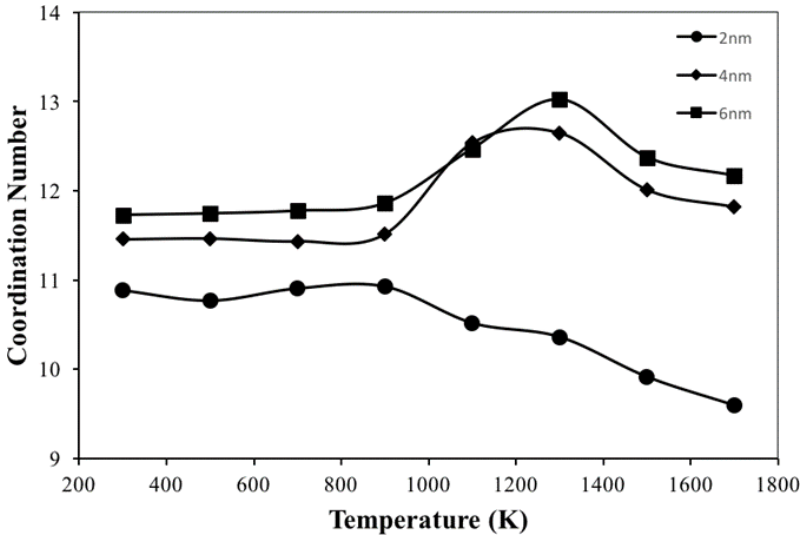

Figure 10. Coordination number change of the amorphous $FeNi_3$ nanoparticle with respect to temperature

According to Figure 10, the coordination number of the amorphous 2 nm particle continuously increased as the temperature approached 300 K, even though it pre- served its amorphous structure during the cooling process. On the other hand, the coordination number of the amorphous nanoparticle with 4 nm diameter reached its maximum value at 1300 K probably because of the sublimation. Then, it stayed at balance around 11 that is very close value with the completely crystalline 4 nm nanoparticle (10.9).

The 6 nm amorphous nanoparticle exhibited a similar trend with the 4 nm nanoparticle, but the coordination number of the 6 nm amorphous nanoparticle reached to 11.2 which is the same coordination value of the initially crystalline 6 nm nanoparticle. This means the initially amorphous nanoparticle with 6 nm diameter completed its crystalline transformation by obtaining same CN value with the initially crystalline nanoparticle.

3.3.Structural evolutions in amorphous $FeNi_3$ NPs

Core-to-surface concentration profiles are essential to observe the atomic movement during heat treatment. The change in the number of Fe and Ni atoms throughout the particles having 2 nm, 4 nm and 6 nm diameter are shown in the following figures. In Figure 11, it is seen that the random mixed atomic patterns of the 2 nm amorphous nanoparticle were preserved as the temperature decreased.

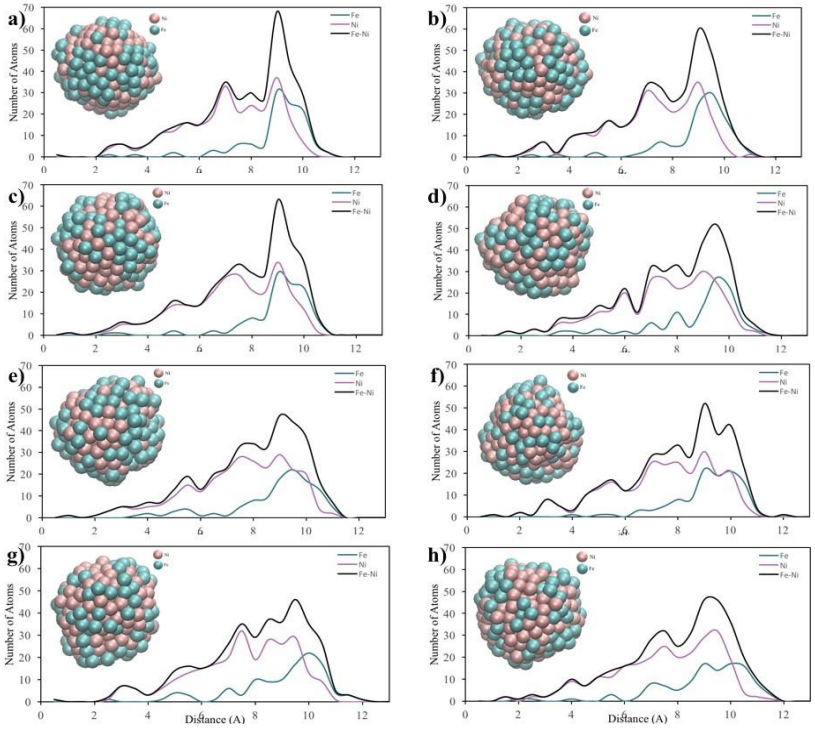

Figure 11. Core-to-surface concentration profiles of Fe and Ni atoms in the 2 nm amorphous nanoparticles at a) 300 K, b) 500 K, c) 700 K, d) 900 K, e) 1100 K, f) 1300 K, g) 1500 K and h) 1700 K

However, Fe atoms diffused from the core to surface, and the initial Fe atomic positions at the core side started to be filled with Ni atoms at lower temperatures. In the end, the main atomic distribution peak of the Fe atoms located at the surface, but Ni atoms spread throughout the particle. From the morphological point of view, it is known that amorphous nanomaterials have unstable structures compared to their crystalline counterparts, so during MD simulations, the shape and surface area of the particles changed to have more stable structures. For example, as the temperature decreased, the irregular shape of the amorphous 2 nm nanoparticle converted to the spherical shape.

According to Figure 12, the melted Fe atoms at the surface stayed during the cooling process and Ni atoms diffused towards the inside of the 4 nm amorphous particle.

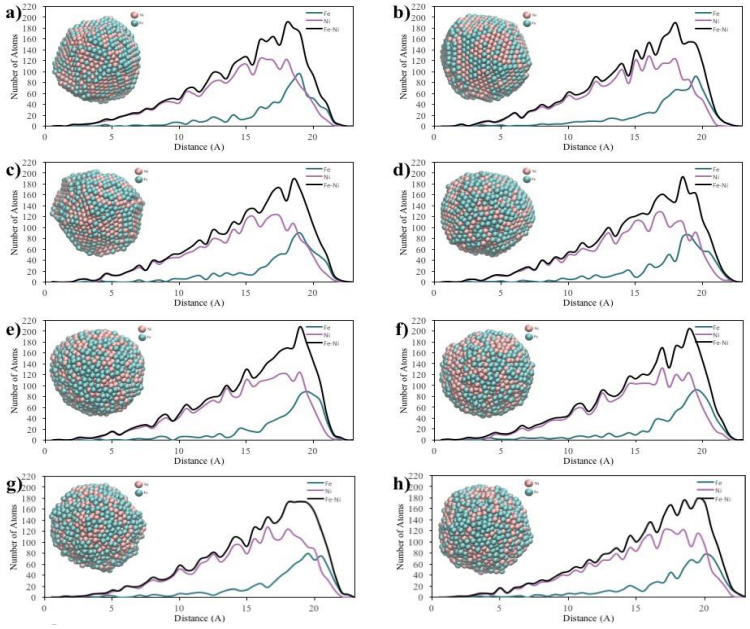

Figure 12. *Core-to-surface concentration profiles of Fe and Ni atoms in the 4 nm amorphous nanoparticles at a) 300 K, b) 500 K, c) 700 K, d) 900 K, e) 1100 K, f) 1300 K, g) 1500 K and h) 1700 K*

Although Ni atoms dominated the core and most of the Fe atoms were located at the surface, the random mixed pattern in the intermediate shell preserved at 300 K. For the 4 nm nanoparticle, it has been observed that the irregular shape of the particles transformed the spherical shape at the onset of the melting; afterward, they reached to a more stable sharp sphere.

In Figure 13, mainly mixed pattern of Fe and Ni atoms obtained at the end of the cooling process, but Ni atoms still dominated the core and melted Fe atoms stayed at the surface, similar to the 4 nm nanoparticle.

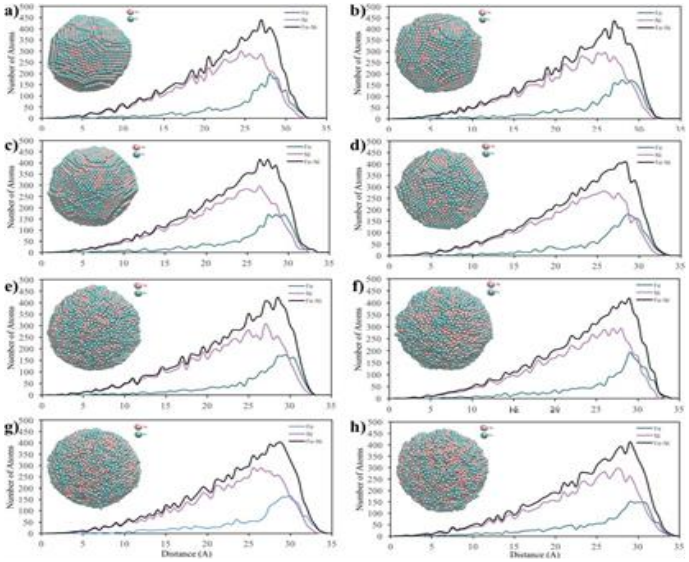

Figure 13. Core-to-surface concentration profiles of Fe and Ni atoms in the 6 nm amorphous nanoparticles at a) 300, K b) 500 K, c) 700 K, d) 900 K, e) 1100 K, f) 1300 K, g) 1500 K and h) 1700 K

Moreover, 6 nm nanoparticle also showed a similar trend with the 4 nm nanoparticle in terms of morphological transformation during the cooling process. With the decreasing temperature, the irregular shape of the 6 nm nanoparticles evaluated smoothly to the spherical shape while melting, and a shape of sharp-sphere was obtained at 300 K which means the 4 nm and 6 nm nanoparticles

had a capability of undergoing a transformation from their initial shapes to geometrically more stable shape.

As it has been explained in the Introduction Section, the difference between atomic sizes of the constituents leads to core-shell structure, in which small atoms are located in the core-side but the bigger ones form an outer shell that surrounds the core. Also, a large difference in the cohesive energy of the atoms causes segregation. In this sys- tem, Fe and Ni atoms have a similar radius and cohesive energy, such as Fe atoms have the 0.126 nm radius with 4.28 eV/atom cohesive energy and Nickel atoms own 0.125 nm radiuses with 4.44 eV/atom cohesive energy [27]. Therefore, the nanoparticles having equal to/larger than 4 nm diameter formed an ordered mixing pattern, rather than segregated or core-shell structure, as it has been expected. Although at room temperature, some Ni atoms stayed at the core side of the smaller particles, as the diameter of the particle size increased to 6 nm, the atomic pattern mainly trans- formed to the ordered mixing pattern and no segregation was observed.

3.4. Voronoi Analysis in crystalline $FeNi_3$ NPs

The Voronoi tessellations of the amorphous nanoparticles with 2 nm, 4 nm and 6 nm diameter at 1700 K and 300 K are shown in Figure 14.

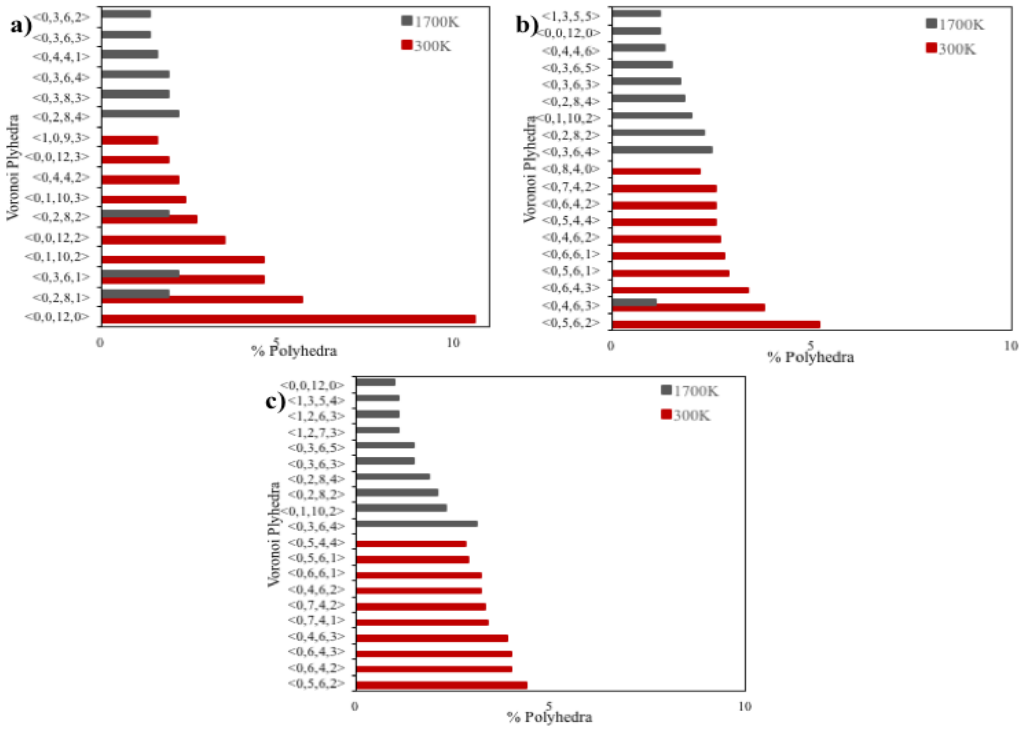

Figure 14. Voronoi analysis of amorphous $FeNi_3$ nanoparticle with a) 2 nm diameter b) 4 nm diameter c) 6 nm diameter

According to Figure 14 (a), none of the polyhedrons in 2 nm amorphous nanoparticle was found in the 2 nm crystalline nanoparticle. This means that amorphous nanoparticle with 2 nm diameter conserved its amorphous structure during the cooling process from 1700 K to 300 K. The vast majority of the Voronoi tessellation of the 2 nm amorphous nanoparticle belonged to <0,0,12,0> polyhedron which showed that the fully icosahedral structure and its deformed forms (<0,1,10,2>, <0,2,8,2>) covered the 2 nm nanoparticle. The other <0,2,8,1> and <0,3,6,1> polyhedral structures

correspond to deformed trigonal prism were also observed in both liquid and solid phase of the 2 nm amorphous nanoparticle.

Due to the fivefold symmetry below the critical sizes, the icosahedral polyhedrons are the stable form of the metallic nanoparticles [28]. However, from the previous studies, it has been shown that the stability of the icosahedral structure decreased when the total number of atoms increased in a nanoparticle [29]. In accordance with the literature, the icosahedral structure <0,0,12,0> disappeared and the trigonal faces decreased to lower than 50% as the size of the particles increased to 4 nm and 6 nm.

According to Figure 14 (b), the main polyhedrons like <0,5,6,2>, <0,6,4,2>, and <0,5,6,1> were found initially amorphous solid nanoparticles having 4 nm diameter. On the other hand, <0,4,6,3> polyhedron structure was observed in both the liquid and the solid phase of the 4 nm amorphous nanoparticle. This means that although 4 nm amorphous and crystalline nanoparticles had some common local atomic arrangement in the solid and liquid phases, the 4 nm nanoparticle with amorphous phase could not completely transformed to the crystalline structure at 300 K.

In Fe-centered Voronoi polyhedra of the 6 nm nanoparticles, Figure 14 (c), it has been observed that all of the local atomic configurations in solid phase were completely different from the liquid phase. Furthermore, most of the polyhedrons in the solid phase were common with the polyhedral shapes of the initially crystalline nanoparticle owing 6 nm diameter in solid phase, such as <0,6,4,2>, <0,5,6,2>, <0,7,4,1>, <0,7,4,2> and <0,5,6,1>. These polyhedrons correspond to the deformed truncated octahedron with its derivatives (tetradecohedron) having $m\bar{3}m$ symmetry. The truncated octahedron is one of the most stable FCC structure because of having the minimum energy for larger nanoparticles [29]. According to the common Voronoi polyhedrons in the 6 nm nanoparticle, it has been seen that the number of rectangular faces of the local polyhedra around Fe atom significantly increased to more than 50% which matched with the distorted FCC lattice structure. Therefore, we can say that the 6 nm amorphous nanoparticle generally transformed to the FCC crystalline lattice structure at 300 K.

Moreover, most of the polyhedron structures in the initially amorphous nanoparticle with 4 nm and 6 nm diameter were common at room temperature, but only a few of them are found in the 2 nm amorphous nanoparticle. This is because 2 nm nanoparticle preserved its amorphous structure throughout the cooling process but the others transformed to the crystalline structure partially or completely. Considering coordination number from the Voronoi analysis, CN of 2 nm amorphous nanoparticle mainly remained higher than 12 which is another proof for the disordered amorphous structure because the amorphous structures may have a more efficient atomic packing [30]. Also, the total coordination numbers of the 6 nm and 4 nm nanoparticles were between 12 and 13 atoms which is consistent with the coordination number of the FCC lattice structure. Therefore, we can conclude that the initial crystalline or amorphous structure did not affect significantly the final FCC structure of the 6 nm nanoparticle at 300 K.

Conclusions

Modeling and simulation study have been performed by means of EAM-MD method in order to investigate the effects of particle size (in 2-6 nm particle size range) and temperature (300-1900 K) on stability and local structural evolutions of equatomic $FeNi_3$ amorphous bulk/nanoalloys at liquid and amorphous solid state. $FeNi_3$ nanosystem was modeled by assuming that, systems with

more than 100 atoms have the same crystal structure as their bulk counterpart. The results of theoretical predictions can be summarized as follows:

1. The three dimensional (3D) atomic configuration of $FeNi_3$ NPs by means of Voronoi analysis reveals that, amorphous nanoparticle with 2 nm diameter conserved its amorphous structure during the cooling process from 1700 K to 300 K. The vast majority of the Voronoi tessellation of the 2 nm amorphous nanoparticle belonged to <0,0,12,0> polyhedron which showed that the fully icosahedral structure and its deformed forms (<0,1,10,2>, <0,2,8,2>) covered the 2 nm nanoparticle. The other <0,2,8,1> and <0,3,6,1> polyhedral structures correspond to deformed trigonal prism were also observed in both liquid and solid phase of the 2 nm amorphous nanoparticle. The main polyhedrons like <0,5,6,2>, <0,6,4,2>, and <0,5,6,1> were found initially amorphous solid nanoparticles having 4 nm diameter. On the other hand, <0,4,6,3> polyhedron structure was observed in both the liquid and the solid phase of the 4 nm amorphous nanoparticle. In Fe-centered Voronoi polyhedra of the 6 nm nanoparticles, it has been observed that all of the local atomic configurations in solid phase were completely different from the liquid phase. Furthermore, most of the polyhedrons in the solid phase were common with the polyhedral shapes of the initially crystalline nanoparticle owing 6 nm diameter in solid phase, such as <0,6,4,2>, <0,5,6,2>, <0,7,4,1>, <0,7,4,2> and <0,5,6,1>. The truncated octahedron is one of the most stable FCC structure because of having the minimum energy for larger nanoparticles and 6 nm amorphous nanoparticle generally transformed to the FCC crystalline lattice structure at 300 K.

2. At high temperatures, there was an absence of an order for all initially amorphous nanoparticles. RDF graphs of the 2 nm nanoparticles reveal that an amorphous structure was preserved during the cooling process even at 300 K. On the other hand, for nanoparticles with 4 nm and 6 nm diameter, there was a transition from amorphous phase to the crystal structure at lower temperatures and at 300 K the complete crystalline structure was obtained in 6 nm nanoparticle with 3.5 Å lattice constant. Although at 300 K, the lattice parameter of both 6 nm and 4 nm nanoparticles reached to 3.5 Å value, the variation in lattice constant of the nanoparticle with 4 nm diameter was higher than for 6 nm diameter because of the size effect on the lattice parameter.

3. Structural analysis on the base of core-to-surface concentration profiles indicated that, the random mixed atomic patterns of the 2 nm amorphous nanoparticle were preserved as the temperature decreased. However, Fe atoms diffused from the core to surface, and the initial Fe atomic positions at the core side started to be filled with Ni atoms at lower temperatures. At the end of cooling process, Fe atoms located at the surface, but Ni atoms spread throughout the particle. During the cooling process of the 4 nm amorphous NP, the melted Fe atoms stayed at the surface and Ni atoms diffused towards the inside of NP. For the 4 nm nanoparticle, it has been observed that the irregular shape of the particles transformed the spherical shape at the onset of the melting; afterward, they reached to a more stable sharp sphere. Although Ni atoms dominated the core and most of the Fe atoms were located at the surface, the random mixed pattern in the intermediate shell preserved at 300 K for 6 nm amorphous NP. Mainly mixed pattern of Fe and Ni atoms obtained at the end of the cooling process, but Ni atoms still dominated the core and melted Fe atoms stayed at the surface, similar to the 4 nm nanoparticle.

4. The coordination number (CN) of the amorphous 2 nm particle continuously increased as the temperature approached 300 K, even though it preserved its amorphous structure during the cooling process. On the other hand, the coordination number of the amorphous nanoparticle with 4 nm

diameter reached its maximum value at 1300 K probably because of the sublimation. Then, it stayed at balance around 11 that is very close value with the completely crystalline 4 nm nanoparticle (10.9). The 6 nm amorphous nanoparticle exhibited a similar trend with the 4 nm nanoparticle, but the coordination number of the 6 nm amorphous nanoparticle reached to 11.2 which is the same coordination value of the initially crystalline 6 nm nanoparticle. This means the initially amorphous nanoparticle with 6 nm diameter completed its crystalline transformation by obtaining same CN value with the initially crystalline nanoparticle.

REFERENCES

[1] Nanoalloys: From Fundamentals to Emergent Applications, ed. F. Calvo, 2-nd edition, 2020; 1-st edition, Elsevier Inc., 2013.

[2] Sh. Moussa, V. Abdelsayed, and M.S. El Shall, Chemical synthesis of metal nanoparticles and nanoalloys, In Nanoalloys, ed. F. Calvo, pp. 1–37, Elsevier Inc., 2013.

[3] Riccardo Ferrando, Julius Jellinek, and Roy L Johnston., Nanoalloys: From Theory to Applications of Alloy Clusters and Nanoparticles, Chem. Rev., 108 (2008) 845–910.

[4] Y. Yao, Ch. Zhang, Y. Fan and J. Zhan, Preparation and microwave absorbing property of porous FeNi powders, Adv. Powd. Tech. 27 (2016) 2285–2290.

[5] V. Solanki, O. I. Lebedev, Md. M. Seikh, N. K. Mahato, B. Raveau, A. K. Kundu, Synthesis and characterization of Co–Ni and Fe–Ni alloy nanoparticles, J. Magn. Magn. Mater. 420 (2016) 39–44.

[6] K. Yatsugi, T. Ishizaki, K. Akedo and M. Yamauchi, Composition-controlled synthesis of solid-solution Fe–Ni nanoalloys and their application in screen-printed magnetic films, J. Nanopart. Res. 21(3) (2019) 60.

[7] P. H. Zhou, L. J. Deng, J. L. Xie, D. F. Liang, L. Chen, and X. Q. Zhao, Nanocrystalline structure and particle size effect on microwave permeability of FeNi powders prepared by mechanical alloying, J. Magn. Magn. Mater. 292 (2005) 325–331.

[8] R. Koohkana, S. Sharafia, H. Shokrollahib and K. Janghorbanb, Preparation of nanocrystalline Fe–Ni powders by mechanical alloying used in soft magnetic composites, J. Magn. Magn. Mater. 320 (2008) 1089–1094.

[9] K. McNamara, S. A. M. Tofail, N. D. Thorat, J.Bauer, J. J. E. Mulvihill, Biomedical applications of nanoalloys, In Nanoalloys, 2-nd edition, ed. F. Calvo, pp. 381-432, Elsevier Inc., 2020.

[10] Z. A. Matysina. A. O. Mekhrabov, Z. M. Babaev, and et al., Impurities in Ni_3Fe Alloys, Phys. Stat. Sol. (b) 138 (1986) 399-406.

[11] A. O. Mekhrabov, Pseudopotential Calculations of Short-Range Atomic Order Characteristics of 3-component Ni_3(Fe, Me) Alloys, Fiz. Metal. Metalloved. 62 (1986) 1023-1025.

[12] A. O. Mekhrabov, Z. M. Babaev, and et al., Pseudopotential Calculations of the Atomic Pair Interaction Energies and Kurnakov Temperature evaluation for Ni_3(Fe, Me) ternary Alloys, Fiz. Metal. Metalloved. 61 (1986) 1089-1093.

[13] Z. A. Matysina, A. O. Mekhrabov, and et al., Impurities in Ni_3Fe Magnetic Alloys, J. Phys. Chem. Sol. 48 (1987) 419-423.

[14] Z. A. Matysina, A. O. Mekhrabov and Z. M. Babaev, Ordering Temperatures and Order Parameters of Ni_3Fe Alloys with Mn and Cr Impurities, Fiz. Metal. Metalloved. 64 (1987) 202-205.

[15] Z. M. Babaev, A. Z. Menshikov, A. O. Mekhrabov, E. S. Valiev, Atomic Ordering in Ni_3(Fe 1-x Mnx) Alloys, Fiz. Metal. Metalloved. 64 (1987) 762-766.

[16] A. O. Mekhrabov, Impurity Effect of Me= Cr, Nb, or Mn Third-Component Atoms on Hyperfine Interactions in Ordered Ni_3Fe Alloys, Hyperfine Interactions 59 (1990), 337-340.
[17] H. P. Cheng and D. E. Ellis., First-principles potentials in modeling structure and thermodynamics of Fe-Ni alloys, Phys. Rev. B 39(17) (1989) 12469–12483.
[18] Y. Mishin, M. J. Mehl, and D. A. Papaconstantopoulos, Phase stability in the Fe-Ni system: Investigation by first-principles calculations and atomistic simulations, Acta Mater. 53(15) (2005) 4029–4041.
[19] T. Halicioglu and C. W. Bauschlicher Jr., Physics of Microclusters, Reports on Progress in Physics 51(6) (1988) 883.
[20] G. Bonny, R. C. Pasianot and L. Malerba, Fe–Ni many-body potential for metallurgical applications, Model. Simul. Mater. Sci. Eng. 17 (2009) 025010.
[21] M. V. Akdeniz and A. O. Mekhrabov, Size dependent stability and surface energy of amorphous FePt nanoalloy, J. of All. Comp. 788 (2019) 787-798.
[22] M. Yalcin, A. O. Mekhrabov and M. V. Akdeniz, Effects of Nanoparticle Geometry and Temperature on the Structural Evolutions in FeCo Nanoalloys, Acta Phys. Pol. A 125(2), (2014) 600-602.
[23] E. Furio, A molecular dynamics primer, Technical report, International School for Advanced Studies (SISSA-ISAS), Trieste, Italy, 1997.
[24] M. E. Tuckerman, J. Alejandre, R. López-Rendón, A. L. Jochim and G. J. Martyna, A Liouville-operator derived measure-preserving integrator for molecular dynamics simulations in the isothermal-isobaric ensemble, J. Phys. A: Mathematical and General, 39(19) (2006) 5629–5651.
[25] I. Chicinas, V. Pop, O. Isnard, J. M. Le Breton and J. Juraszek. Synthesis and magnetic properties of Ni_3Fe intermetallic compound obtained by mechanical alloying. Journal of Alloys and Compounds, 352(1-2):34–40, 2003
[26] W. H. Qi, B. Y. Huang, M. P. Wang, Z. M. Yin, and J. Li. Molecular dynamic simulation of the size- and shape-dependent lattice parameter of small Platinum nanoparticles. Journal of Nanoparticle Research, 11(3):575–580, 2009
[27] P. H. T. Philipsen and E. J. Baerends, Cohesive energy of 3d transition metals: Density functional theory atomic and bulk calculations, Physical Review B, 54(8):5326–5333, 1996.
[28] M. Hanbücken, P. Müller and R.B. Wehrspohn, Mechanical Stress on the Nanoscale: Simulation, Material Systems and Characterization Techniques. Wiley, 2011.
[29] S. Ali, V. S. Myasnichenko and E. C. Neyts, Size-dependent strain and surface energies of gold nanoclusters, Phys. Chem. Chem. Phys., 18(2):792–800, 2016.
[30] D. Bazin, I. Fechete, F. C. Garin, Giovanni Barcaro, F. R. Negreiros, L. Sementa and A. Fortunelli, Reactivity and catalysis by nanoalloys, In Nanoalloys, ed. F. Calvo, pp. 283–344, Elsevier Inc., 2013.

Received: 15.05.2023
Accepted: 30.10.2023